NANO LETTERS

LETTER

pubs.acs.org/NanoLett

Multispectral Plasmon Induced Transparency in Coupled Meta-Atoms

Alp Artar,[†] Ahmet A. Yanik,[†] and Hatice Altug*

Electrical and Computer Engineering Department, Boston University, Boston, Massachusetts 02215, United States

Supporting Information

ABSTRACT: We introduce an approach enabling construction of a scalable metamaterial media supporting multispectral plasmon induced transparency. The composite multilayered media consist of coupled meta-atoms with radiant and subradiant hybridized plasmonic modes interacting through the structural asymmetry. A perturbative model incorporating hybridization and mode coupling is introduced to explain the observed novel spectral features. The proposed scheme is demonstrated experimentally by developing a lift-off-free fabrication scheme that can automatically register multiple metamaterial layers in the transverse plane. This metamaterial which can simultaneously enhance nonlinear processes at multiple frequency domains could open up new possibilities in optical information processing.

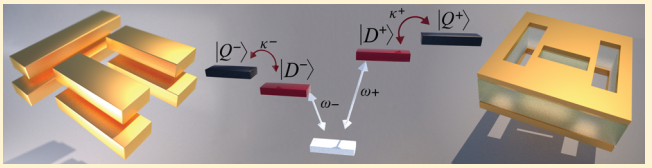

KEYWORDS: Metamaterials, electromagnetically induced transparency, plasmons, plasmon hybridization, Fano resonances, strong coupling

Electromagnetically induced transparency (EIT), a spectrally narrow optical transmission window accompanied with extreme dispersion, results from quantum interference of multiple excitation pathways through short and long-lived resonances.[1] Within this spectral window, dramatically slowed down photons and orders of magnitude enhanced nonlinearities can enable manipulation of light at few-photon power levels.[2] Historically, EIT has been implemented in laser-driven atomic quantum systems. However, limited material choices and stringent requirements to preserve the coherence of excitation pathways in atomic systems have significantly constrained the use of EIT effect.[3]

Recent studies have revealed that EIT-like optical responses can be obtained classically using on-chip plasmonic and photonic nanoresonators.[4−20] Much of the research effort so far focused on isolated meta-atoms (either photonic or plasmonic) showing EIT-like effect at a single resonance. On the other hand, metamaterial systems supporting EIT-like optical responses at multiple-spectral windows can simultaneously enhance multicolored photon−photon interactions and open up new possibilities in nonlinear optics and optical information processing.[21−23]

In this Letter, we propose and demonstrate a novel approach based on coupled meta-atoms to construct a homogeneous and scalable medium supporting multispectral EIT-like effect (plasmon induced transparency). The proposed structure consists of a two slot antenna based complementary metamaterial layers with a small gap (dielectric layer thickness) enabling strong near-field interaction in between. Each planar metamaterial layer has bright (radiant) and dark (subradiant) plasmonic modes coupled through the structural asymmetry ($s \neq 0$) in an analogy to transition-allowed and -forbidden atomic orbitals coupled through a common excited state.[6] As shown in Figure 1b (blue curve), isolated meta-atoms on a single-layer metamaterial exhibit an EIT-like reflection[10] with spectral features that are controlled by the artificial atomic orbitals (plasmonic modes). Once stacked in a multilayered structure (Figure 1b, black curve), presence of strong near-field coupling between the meta-atoms causes splitting of the EIT resonances and leads to multispectral EIT-like behavior. The underlying physical principles for this phenomenon are related to plasmonic hybridization effects[24] and dark-bright mode couplings of the in-phase and out-phase hybridized states. To explain these novel spectral features, we introduce a perturbative model incorporating hybridization and mode coupling. Furthermore, we experimentally demonstrate the proposed scheme by developing a lift-off free fabrication scheme that can simultaneously register multiple metamaterial layers in the third dimension.

In the following, we start by describing the perturbative model that provides insight into the physical processes involved in these structures. For the double layered metamaterial, a total Hamiltonian can be defined as

$$H^{\mathrm{T}} = \tilde{H}_0 + \tilde{H}_0' + \tilde{K} + \tilde{\Sigma}$$

Here, $\tilde{H}_0$ and $\tilde{H}_0'$ are the 2×2 unperturbed Hamiltonians of the isolated metamaterial layers defined in a basis set consisting of decoupled bright (dipolar) and dark (quadrupole) modes in the absence of a structural asymmetry ($s \neq 0$). The weak interactions between the bright and the dark modes

Received: January 18, 2011
Revised: March 4, 2011

dx.doi.org/10.1021/nl200197j | *Nano Lett.* XXXX, XXX, 000–000

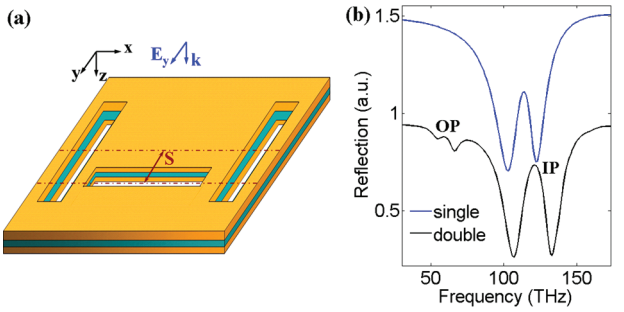

Figure 1. (a) Geometry of the multilayered metamaterial. Structure consists of two Au layers (30 nm thickness) that are separated by a dielectric (SiN_x) layer (70 nm thickness). Each layer has a dipole and a quadrupole slot antenna (all slot antennas have 700 nm length, 100 nm width). The small in-plane separation between the dipolar and quadrupolar antennas is 50 nm on both sides and periods are 1200 nm on both x and y directions. Parameter s is defined as the offset of the dipolar antenna from the geometrical center of the structure. Blue arrows show the configuration of the incident light. (b) Simulated reflection spectra for asymmetric ($s \neq 0$) single- and double-layered structures are shown (with an offset for clarity). Multispectral EIT-like response (in-phase and out-of-phase) is observable with double-layered metamaterial.

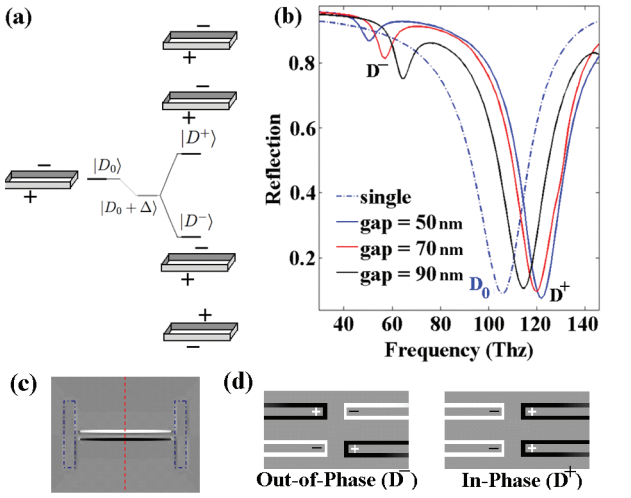

Figure 2. (a) Hybridization scheme for the dipolar mode. (b) Tuning of the spectra with the dielectric layer thickness is shown for the symmetric structure ($s = 0$). As the dielectric layer thickness reduces, splitting of energy between the hybrid modes increases. Single layer spectrum is shown with the blue dashed curve. Splitting energies ($2\varepsilon_D$) are 202, 260, 297 meV and energy offsets (Δ_D) are 60, 68, 78 meV for gap sizes (dielectric layer thicknesses) of 90, 70, 50 nm, respectively. (c) Charge distribution at the air/metal interface (top view), demonstrating the dipolar mode excitation. This charge distribution is acquired from in-phase state $|D^+\rangle$ of the multilayered structure; however the out-of-phase state $|D^-\rangle$ and also the single-layered dipolar state $|D_0\rangle$ have the exact same charge distribution (not shown). (d) Charge distributions of the hybrid dipolar modes acquired from a multilayered structure with a dielectric layer thickness of 50 nm (cross-sectional view) are shown at a position marked with the red dashed line in (c).

are incorporated with the perturbative Hamiltonian $\tilde{K}$, when a structural asymmetry is introduced ($s \neq 0$). Interactions between the two metamaterial layers are included through the strong near-field coupling Hamiltonian $\tilde{\Sigma}$. Accordingly, the total Hamiltonian for the coupled meta-atoms is given as

$$H^{\mathrm{T}} = \tilde{H}_0 + \tilde{H}_0{}' + \tilde{K} + \tilde{\Sigma} = \begin{matrix}\langle 1| \\ \langle 2|\end{matrix} \begin{bmatrix} H_0 + \mathrm{K} & \Sigma \\ \Sigma^* & H_0{}' + \mathrm{K}' \end{bmatrix} \begin{matrix} \\ |1\rangle \quad |2\rangle \end{matrix} = \begin{matrix}\langle D_0| \\ \langle Q_0| \\ \langle D_0{}'| \\ \langle Q_0{}'|\end{matrix} \begin{bmatrix} E_{D_0} & \kappa & \tau_{\mathrm{inter},D} & \chi' \\ \kappa^* & E_{Q_0} & \chi & \tau_{\mathrm{inter},Q} \\ \tau_{\mathrm{inter},D} & \chi^* & E_{D_0'} & \kappa' \\ (\chi')^* & \tau_{\mathrm{inter},Q} & (\kappa')^* & E_{Q_0'} \end{bmatrix} \begin{matrix} \\ |D_0\rangle \quad |Q_0\rangle \quad |D_0{}'\rangle \quad |Q_0{}'\rangle \end{matrix} \tag{1}$$

where $|1\rangle$ and $|2\rangle$ represent the top and bottom metamaterial layers, respectively. The eigenvalues of the bright ($|D_0\rangle$) and the dark ($|Q_0\rangle$) modes of the isolated metamaterials are defined as E_{D_0} and E_{Q_0}. For clarity, eigenstates and eigenvalues of the second layer are denoted with primes, even for structurally symmetric layers. κ and κ' are due to the weak intralayer coupling among the dark and bright modes in each layer. $\tau_{\mathrm{inter},D}$ and $\tau_{\mathrm{inter},Q}$ are the strong interlayer coupling terms for the bright and dark modes, respectively. χ and χ' are the cross couplings among the bright and dark modes of different layers (interlayer). An important consideration in our analysis is that χ and χ', the cross couplings among the bright and dark modes, are weak and can be neglected. Validity of this assumption will be justified in the following by benchmarking our analytical relations with numerical simulations and experimental measurements. For a metamaterial system where the individual layers have identical structural characteristics, the Hamiltonian terms for both layers are identical ($\kappa = \kappa'$, $\tau_{\mathrm{inter},D/Q} = \tau_{\mathrm{inter},D'/Q'}$, $E_{D_0/Q_0} = E_{D_0'/Q_0'}$). After a simple rearrangement of the matrix elements and a unitary transformation, the total Hamiltonian can be rewritten as in

$$H^T_{\mathrm{hyb}} = \hat{U}[H^{\mathrm{T}}]\hat{U}^* = \begin{matrix}\langle D^+| \\ \langle D^-| \\ \langle Q^+| \\ \langle Q^-|\end{matrix} \begin{bmatrix} E_{D_0} + \Delta_D + \varepsilon_D & 0 & \kappa & 0 \\ 0 & E_{D_0} + \Delta_D - \varepsilon_D & 0 & \kappa \\ \kappa^* & 0 & E_{Q_0} + \Delta_Q + \varepsilon_Q & 0 \\ 0 & \kappa^* & 0 & E_{Q_0} + \Delta_Q - \varepsilon_Q \end{bmatrix} \begin{matrix} \\ |D^+\rangle \quad |D^-\rangle \quad |Q^+\rangle \quad |Q^-\rangle \end{matrix} \tag{2}$$

in an orthogonal basis set consisting of

$$|D^{\pm}\rangle = \frac{1}{\sqrt{2}}[|D_0\rangle \pm |D_0{}'\rangle] \tag{3a}$$

$$|Q^{\pm}\rangle = \frac{1}{\sqrt{2}}[|Q_0\rangle \pm |Q_0{}'\rangle] \tag{3b}$$

dx.doi.org/10.1021/nl200197j |Nano Lett. XXXX, XXX, 000–000

diagonalizing the Hamiltonian $H^T_{s=0} = \tilde{H}_0 + \tilde{H}_0{}' + \tilde{\Sigma}$ (when the system is symmetric $s = 0$) in the strong coupling regime ($|E_{D_0} - E_{D_0'}| \ll 2\tau_{\text{inter},D}$ and $|E_{Q_0} - E_{Q_0'}| \ll 2\tau_{\text{inter},Q}$). These hybrid eigenstate pairs are in-phase (+) and out-of phase (−) superpositions of the isolated layer eigenmodes of the structurally symmetric multilayer system ($s = 0$). The associated energies of the dipolar hybrid modes are, $E^{\pm}_D = E_{D_0} + \Delta_D \pm \varepsilon_D$, where the offset term is $\Delta_D = \langle D_0|\tau_{\text{inter},D}|D_0\rangle$ and the splitting term is $\varepsilon_D = \langle D_0|\tau_{\text{inter},D}|D_0'\rangle$ (a similar set can be obtained for quadrupole modes). Since off diagonal terms in the transformed Hamiltonian H^T_{hyb} are much weaker than the diagonal terms, the off-diagonal matrix elements κ and κ' are treated as the elements of the perturbative Hamiltonian introduced by the structural asymmetry ($s \neq 0$). Using the transformed Hamiltonian H^T_{hyb}, a set of coupled Lorentzian oscillator relations can be derived in an analogy to atomistic EIT resonances.

Initially, the hybridization of eigenstate pairs in the form of in-phase (+) and out-of phase (−) superpositions of the isolated layer eigenmodes is shown in Figure 2 for the structurally symmetric multilayer system ($s = 0$ and $\kappa = 0$) using finite difference time-domain (FDTD) analysis. For a single-layered metamaterial, only the resonance dip corresponding to the excitation of the dipolar bright mode is observable in the reflection spectrum (Figure 2(b), dashed blue curve). For the double layered metamaterial, two resonance dips appear corresponding to in-phase and out-of-phase hybridized modes due to the degeneracy breaking as given in eq 3a (solid curves in Figure 2b). The mode energies and the splitting in between are controlled by the strength of the interlayer coupling of the metamaterial layers. As predicted by our Hamiltonian treatment, smaller gaps (dielectric layer thicknesses) lead to larger energy splittings as this coupling becomes stronger (Figure 2b). The in-phase and out-of-phase character of these hybridized states are also confirmed with FDTD simulations showing cross-sectional charge distributions of the dipolar modes (Figure 2d). The in-phase hybrid mode is radiant as a result of its overall dipolar character. The radiant out-of-phase mode is harder to excite with respect to the in-phase mode, due to the partial cancellation of the dipolar moments of the subsequent layers. Nevertheless, resonance dip corresponding to the out-of-phase mode is still observable due to the retardation effects (Figure 2b, solid curves). In Figure 2b, resonances due to hybridized quadrupolar modes are not observable, since any linear combination of the subradiant quadrupolar modes of the isolated structures is also subradiant. Structural symmetry must be broken for the excitation of these quadrupolar hybridized modes.

Breaking the symmetry of the multilayered structure ($s \neq 0$) leads to near-field coupling between the dark and bright modes ($\kappa \neq 0$) and results in the excitation of the dark modes with the perpendicularly incident light. Indirect excitation of these hybrid quadrupolar dark modes leads to multispectral EIT-like behavior (Figure 3 black curve). Charge distribution of the out-of-phase (OP) EIT resonance at the top surface (Figure 3a inset), indicates strong coupling of the external driving field to this mode. A similar charge distribution is also observed for the in-phase (IP) EIT resonance (not shown). Cross sectional charge distributions of the quadrupolar modes (Figure 3b) confirm the in-phase and out-of-phase mode characters. Full spectral response of the multilayered structure can be understood following our perturbative Hamiltonian approach. Here, a coupled Lorentzian oscillator model is derived from the transformed Hamiltonian H^T_{hyb} in a similar way to the EIT concepts in atomic physics. In our analysis, the following three observations are employed. (i) Breaking of the structural symmetry ($s \neq 0$) results in weak near-field coupling of the hybridized dark and bright modes, an effect which can be incorporated to the unperturbative Hamiltonian ($s = 0$) with the perturbative terms κ and κ'. (ii) There is no direct coupling between the in-phase and out-of-phase hybrid modes, due to the large energy difference in between ($D^{\pm} \leftrightarrow Q^{\mp}$). (iii) Damping rates of the quadrupole ($\gamma^{\pm}_Q$) and dipole ($\gamma^{\pm}_D$) hybrid modes are small enough that the condition $\gamma^{\pm}_Q \ll \gamma^{\pm}_D \ll \omega_{\pm}$ is satisfied. Here $\omega_{\pm}$ are the resonant frequencies of the in-phase and out-of-phase hybrid pairs ($\omega_{\pm} = E^{\pm}_D/\hbar \approx E^{\pm}_Q/\hbar$).

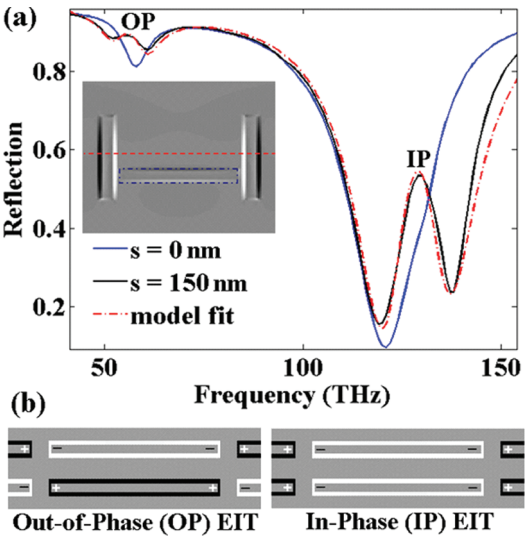

Figure 3. (a) Asymmetric (s = 150 nm) and symmetric (s = 0 nm) double-layer EIT-like spectra. Two dips seen in the symmetric structure's spectrum corresponds to hybrid dipolar modes as in Figure 2b. Asymmetric structure shows two EIT-like peaks at different spectral positions. A model fit based on Lorentzian harmonic oscillators is shown for the double-layered structure (red dashed curve with $\kappa^- = 12$ THz, $\kappa^+ = 23$ THz),[25] which traces the calculated spectra very well. A genetic search algorithm is implemented to extract the parameters using a least-squares sum fit. Calculated group indices for the in-phase and out-of-phase modes are $n_g^+ = 16$, $n_g^- = 9.3$. These values can be optimized by adjusting the coupling terms $\kappa^{\pm}$. Inset shows the top view charge distribution at the air/metal interface for the out-of-phase EIT peak (in-phase EIT peak also shows the same distribution). Stronger excitation of the quadrupolar mode is shown. (b) Cross-sectional charge distributions of the quadrupolar antennas are shown at a position marked with the red dashed line in the inset. Hybridization of the quadrupolar resonance is shown.

We can express all hybrid states in the form of $|\phi\rangle = \tilde{\phi}e^{i\omega t}$ (where ϕ is $Q^{\pm}$ and $D^{\pm}$) and denote the external driving field as $\tilde{E}_0 e^{i\omega t}$. Then, in agreement with the total Hamiltonian of the system, the following set of linear equations is obtained for the coupled Lorentzian oscillators

$$\begin{bmatrix} \omega - \omega_+ + i\gamma_D^+ & \kappa^+ & 0 & 0 \\ \kappa^+ & \omega - \omega_+ - \delta^+ + i\gamma_Q^+ & 0 & 0 \\ 0 & 0 & \omega - \omega_- + i\gamma_D^- & \kappa^- \\ 0 & 0 & \kappa^- & \omega - \omega_- - \delta^- + i\gamma_Q^- \end{bmatrix} \begin{bmatrix} \tilde{D}^+ \\ \tilde{Q}^+ \\ \tilde{D}^- \\ \tilde{Q}^- \end{bmatrix} = \begin{bmatrix} g^+\tilde{E}_0 \\ 0 \\ g^-\tilde{E}_0 \\ 0 \end{bmatrix} \quad (4)$$

dx.doi.org/10.1021/nl200197j |Nano Lett. XXXX, XXX, 000–000

Here $\kappa^{\pm}$ values are the coupling parameters of the perturbative term for the in-phase and out-of-phase hybrid pairs, which are determined by the structural offset "s". $\delta^{\pm}$ values are the small detuning of the frequencies of in-phase and out-of-phase hybrid mode pairs ($\delta^{\pm} = (E_D^{\pm} - E_Q^{\pm})/\hbar$). $g^{\pm}$ values are the geometrical parameters that define the coupling efficiency of the dipolar hybrid modes ($D^{\pm}$) to the external field. Equation 4 represents two coupled Lorentzian oscillator pairs corresponding to in-phase and out-of-phase hybridized modes of the whole structure. The external field (E_0) drives the bright modes in each meta-atom, which are subsequently coupled to the dark modes (through $\kappa^{\pm}$). With these equations the amplitudes of the dipolar hybrid states ($D^{\pm}$) can be derived as

$$\tilde{D}^{\pm} = \frac{-g^{\pm}\tilde{E}_0(\omega - \omega_{\pm} - \delta^{\pm} + i\gamma_Q^{\pm})}{(\omega - \omega_{\pm} + i\gamma_D^{\pm})(\omega - \omega_{\pm} - \delta^{\pm} + i\gamma_Q^{\pm}) - (\kappa^{\pm})^2} \quad (5)$$

The complex amplitudes of the corresponding modes (given in eq 5) are directly proportional to the polarizability of the modes, which governs the spectral characteristics of the plasmonic structure. The overall spectral response is given by the superposition of these amplitudes. The close agreement between this analytical derivation and the FDTD analysis confirms the validity of our perturbative model as shown in Figure 3a (dashed curve). The physical principles leading to multispectral EIT-like behavior can be equivalently observed in other structures. As an example, we implemented our approach with multilayered *dolmen structures*,[6] and obtained a clear multispectral EIT-like behavior (see Supporting Information).

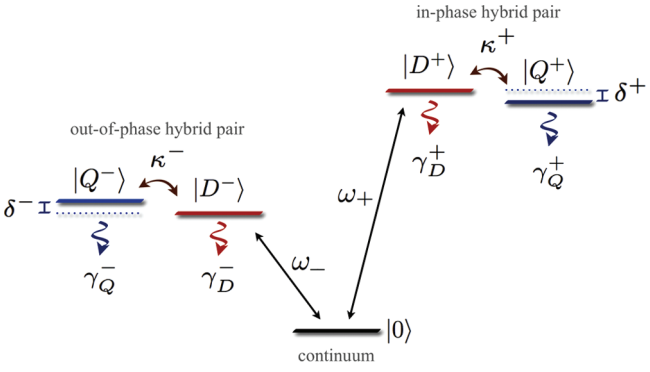

Figure 4. Coupled three-level system model for multispectral plasmon induced transparency. Coupled meta-atoms have four states which form a five-level system with the continuum.

Equation 5 is in close analogy to atomic physics, where the investigated atomic absorption cross section are given with a similar formula.[1] This analogy allows us to illustrate multispectral EIT phenomena in our composite structure with five-level state diagram as shown in Figure 4. It is important to note that these eigenstates are strongly correlated, since they are a linear combination of the same basis sets (D_0,Q_0) as shown in the hybridization diagram in Figure 2a.

Experimental verification of this novel phenomenon is demonstrated using a lift-off free fabrication method that results in simultaneous patterning of multilayered slot antennas.[26] In our fabrication scheme, we start with a free-standing membrane, which is patterned with nanoapertures using e-beam lithography and dry-etching.[27,28] Subsequent metal deposition on both sides with a highly directional e-beam evaporation results in multiple stacks that are automatically registered with respect to each other in the *xy*-plane. Similarly, this fabrication scheme can be extended to fabricate devices with an even larger number of layers.[29] Cross-sectional scanning electron microscope (SEM) image of the final structure shows negligible metal covering at the inner side walls (inset to Figure 5d). Spectral data collection is done with a Bruker IFS 66/s Fourier transform infrared (FTIR) spectrometer with a Hyperion 1000 IR microscope in reflection mode. In measurements obtained from the single-layered structure, a clear EIT-like spectral response is observed at a single frequency (~100 THz, Figure 5c). On the other hand, experimental measurements obtained from the double-layered structure reveal two EIT peaks as predicted by the analytical relations (Figure 5d). The length of the dipolar slot antenna is 700 nm, and its width is 125 nm. The quadrupolar antenna lengths are 900 nm with a same width of 125 nm. The small in-plane separation between the dipolar and the quadrupolar antenna is 60 nm. The thicknesses of the deposited gold films are 30 nm on both sides with a dielectric layer of 70 nm in between. A structural asymmetry (s) of 135 nm is introduced to enable the excitation of hybrid quadrupolar modes.

In conclusion, we presented a method to extend the EIT-like phenomena to multiple spectral positions by tailoring the near-field

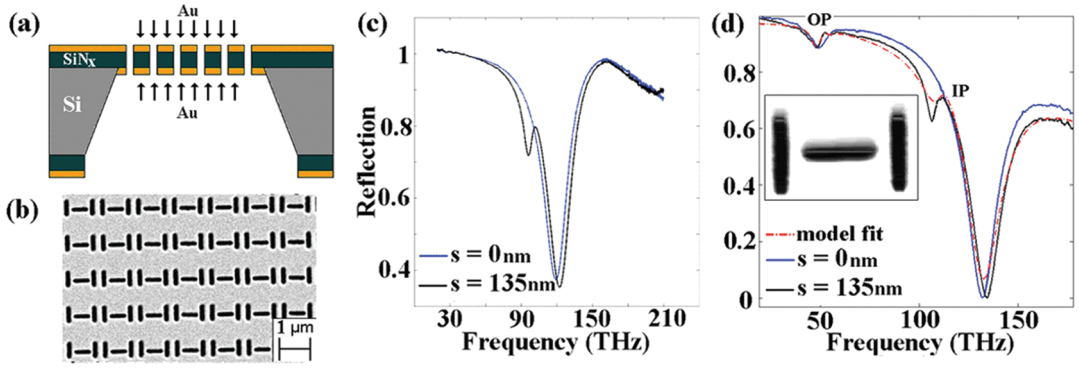

Figure 5. (a) Illustration of the double-layered structure fabrication on a free-standing membrane. (b) SEM image of an array is shown. Reflection spectra of the symmetric ($s = 0$) and asymmetric ($s \neq 0$) for (c) single-layered and (d) double-layered structures are shown. A model fit based on Lorentzian harmonic oscillators is shown for the double-layered asymmetric structure's spectrum (red dashed curve with $\kappa^- = 9.7$ THz, $\kappa^+ = 27.4$ THz).[30] The dipolar slot antenna length is 700 nm and the quadrupolar antenna lengths are 900 nm, all antenna widths are kept at 125 nm. The gap between the dipolar and quadrupolar antennas is 60 nm. Periods are 1200 nm on both *x* and *y* directions. Both Au layers are 30 nm with a 70 nm dielectric layer in-between. Inset in (d) shows the cross section image of the double-layered structure. Coverage of the sidewalls due to the metal deposition is minimal.

dx.doi.org/10.1021/nl200197j |*Nano Lett.* XXXX, XXX, 000–000

coupling of meta-atoms in a multilayered metamaterial system. In particular, two near-field interaction mechanisms make this phenomena possible; (i) hybridization of plasmonic resonances ($\tilde{\Sigma}$) and (ii) interaction between the bright and dark antennas ($\tilde{K}$). The method is demonstrated experimentally and theoretically with planar slot antenna based multilayered metamaterial systems. For experimental demonstration, a lift-off free fabrication scheme that can simultaneously register multiple metamaterial layers is introduced. The provided analytical investigations are kept general. Therefore, our method can be easily extended to other antenna geometries[31] (see Supporting Information) as well as scaled to a larger number of metamaterial layers.

■ ASSOCIATED CONTENT

Supporting Information. Additional information regarding electric field distributions and enhancements at plasmon induced reflection peaks and multispectral plasmon induced transparency with nanoparticles. This material is available free of charge via the Internet at http://pubs.acs.org.

■ AUTHOR INFORMATION

Corresponding Author

*E-mail: altug@bu.edu.

Author Contributions

†These authors contributed equally

■ ACKNOWLEDGMENT

This work is supported in part by NSF CAREER Award (ECCS-0954790), ONR Young Investigator Award, Massachusetts Life Science Center New Investigator Award, NSF Engineering Research Center on Smart Lighting (EEC-0812056), Boston University Photonics Center, and Army Research Laboratory.

■ REFERENCES

(1) Boller, K. J.; Imamoglu, A.; Harris, S. E. Observation of electromagnetically induced transparency. *Phys. Rev. Lett.* **1991**, *66*, 2593–2596.

(2) Harris, S. E.; Field, J. E.; Imamoglu, A. Nonlinear optical processes using electromagnetically induced transparency. *Phys. Rev. Lett.* **1990**, *64*, 1107–1110.

(3) Liu, C.; Dutton, Z.; Behroozi, C. H.; Hau, L. V. Observation of coherent optical information storage in an atomic medium using halted light pulses. *Nature* **2001**, *409*, 490–493.

(4) Yanik, M. F.; Fan, S. Stopping light all optically. *Phys. Rev. Lett.* **2004**, *92*, No. 083901.

(5) N. Papasimakis, N.; Fedotov, V. A.; Zheludev, N. I.; Prosvirnin, S. L. Metamaterial analog of electromagnetically induced transparency. *Phys. Rev. Lett.* **2008**, *101*, No. 253903.

(6) Zhang, S.; Genov, D. A.; Wang, Y.; Liu, M.; Zhang, X. Plasmon-induced transparency in metamaterials. *Phys. Rev. Lett.* **2008**, *101*, No. 047401.

(7) Liu, N.; Langguth, L.; Weiss, T.; Kastel, J.; Fleischhauer, M.; Pfau, T.; Giessen, H. Plasmonic analogue of electromagnetically induced transparency at the Drude damping limit. *Nat. Mater.* **2009**, *8*, 758–762.

(8) Shvets, G.; Wurtele, J. S. Transparency of magnetized plasma at the cyclotron frequency. *Phys. Rev. Lett.* **2002**, *89*, No. 115003.

(9) Luk'yanchuk, B.; Zheludev, N. I.; Maier, S. A.; Halas, N. J.; Nordlander, P.; Giessen, H.; Chong, C. T. The Fano resonance in plasmonic nanostructures and metamaterials. *Nat. Mater.* **2010**, *9*, 707–715.

(10) Liu, N.; Weiss, T.; Mesch, M.; Langguth, L.; Eigenthaler, U.; Hirscher, M.; Sonnichsen, C.; Giessen, H. Planar metamaterial analogue of electromagnetically induced transparency for plasmonic sensing. *Nano Lett.* **2009**, *10*, 1103–1107.

(11) Zia, R.; Schuller, J.; Chandran, A.; Brongersma, M. Plasmonics: the next chip-scale technology. *Mater. Today* **2006**, *9*, 20–27.

(12) Hao, F.; Sonnefraud, Y.; Dorpe, P. V.; Maier, S. A.; Halas, N. J.; Nordlander, P. Symmetry breaking in plasmonic nanocavities: Subradiant LSPR sensing and a tunable Fano resonance. *Nano Lett.* **2008**, *8*, 3983–3988.

(13) Verellen, N.; Sonnefraud, Y.; Sobhani, H.; Hao, F.; Moshchalkov, V. V.; Dorpe, P. V.; Nordlander, P.; Maier, S. A. Fano resonances in individual coherent plasmonic nanocavities. *Nano Lett.* **2009**, *9*, 1663–1667.

(14) Mirin, N. A.; Bao, K.; Nordlander, P. Fano resonances in plasmonic nanoparticle aggregates. *J. Phys. Chem. A* **2009**, *113*, 4028.

(15) Fan, J. A.; Wu, C.; Bao, K.; Bao, J.; Bardhan, R.; Halas, N. J.; Manoharan, V. N.; Nordlander, P.; Shvets, G.; Capasso, F. Self-assembled plasmonic nanoparticle clusters. *Science* **2010**, *328*, 1135–1138.

(16) Lassite, J. B.; Sobhani, H.; Fan, J. A.; Kundu, J.; Capasso, F.; Nordlander, P.; Halas, N. J. Self-assembled plasmonic nanoparticle clusters. *Nano Lett.* **2010**, *10*, 3184–3189.

(17) Hao, F.; Nordlander, P.; Sonnefraud, Y.; Dorpe, P. V.; Maier, S. A. Tunability of subradiant dipolar and Fano-type plasmon resonances in metallic ring/disk cavities: implications for nanoscale optical sensing. *ACS Nano* **2009**, *3*, 643–652.

(18) Hentschel, M.; Saliba, M.; Vogelgesang, R.; Giessen, H.; Alivisatos, A. P.; Liu, N. Transition from isolated to collective modes in plasmonic oligomers. *Nano Lett.* **2010**, *10*, 2721–2726.

(19) Evlyukhin, A. B.; Bozhevolnyi, S. I.; Pors, A.; Nielsen, M. G.; Radko, I. P.; Willatzen, M.; Albrektsen, O. Detuned electrical dipoles for plasmonic sensing. *Nano Lett.* **2010**, *10*, 4571–4577.

(20) Mukherjee, S.; Sobhani, H.; Lassiter, J. B.; Bardhan, R.; Nordlander, P.; Halas, N. Fanoshells: Nanoparticles with built-in Fano resonances. *Nano Lett.* **2010**, *10*, 2694–2701.

(21) Kekatpure, R. D.; Barnard, E. S.; Cai, W.; Brongersma, M. Phase-coupled plasmon-induced transparency. *Phys. Rev. Lett.* **2010**, *104*, No. 243902.

(22) Xu, Q.; Sandhu, S.; Povinelli, M. L.; Shakya, J.; Fan, S.; Lipson, M. Experimental realization of an on-chip all-optical analogue to electromagnetically induced transparency. *Phys. Rev. Lett.* **2006**, *96*, No. 123901.

(23) Lukin, M. D.; Imamoglu, A. Nonlinear optics and quantum entanglement of ultraslow single photons. *Phys. Rev. Lett.* **2000**, *84*, 1419–1422.

(24) Prodan, E.; Radloff, C.; Halas, N. J.; Nordlander, P. A hybridization model for the plasmon response of complex nanostructures. *Science* **2003**, *302*, 419–422.

(25) Other used model parameters are, $\omega_+/\omega_- = 128/57$ THz, $\delta_+/\delta_- = 0.9/-0.8$ THz, $\gamma_Q^+/\gamma_Q^- = 8.32/6.1$ THz, $\gamma_D^+/\gamma_D^- = 30.7/17.7$ THz.

(26) Yanik, A. A.; Huang, M.; Artar, A.; Chang, T. Y.; Altug, H. Integrated nanoplasmonic-nanofluidic biosensors with targeted delivery of analytes. *Appl. Phys. Lett.* **2010**, *96*, No. 021101.

(27) Aksu, S.; Yanik, A. A.; Adato, R.; Artar, A.; Huang, M.; Altug, H. High-throughput nanofabrication of infrared plasmonic nanoantenna arrays for vibrational nanospectroscopy. *Nano Lett.* **2010**, *10*, 2511–2518.

(28) Artar, A.; Yanik, A. A.; Altug, H. Fabry-Perot nanocavities in multilayered plasmonic crystals for enhanced biosensing. *Appl. Phys. Lett.* **2009**, *95*, No. 051105.

(29) Valentine, J.; Zhang, S.; Zentgraf, T.; Ulin-Avila, E.; Genov, D. A.; Bartal, G.; Zhang, X. Three-dimensional optical metamaterial with a negative refractive index. *Nature* **2008**, *455*, 376–379.

(30) Other used model parameters are, $\omega_+/\omega_- = 131/50$ THz, $\delta_+/\delta_- = 14.9/4.8$ THz, $\gamma_Q^+/\gamma_Q^- = 12.19/4.49$ THz, $\gamma_D^+/\gamma_D^- = 45.7/11.9$ THz.

(31) Cubukcu, E.; Kort, E. A.; Crozier, K. B.; Capasso, F. Plasmonic laser antenna. *Appl. Phys. Lett.* **2006**, *89*, 093120-22.